JEE Journal of Ecological Engineering

Journal of Ecological Engineering 2023, 24(8), 12–24
https://doi.org/10.12911/22998993/163174
ISSN 2299–8993, License CC-BY 4.0

Received: 2023.03.14
Accepted: 2023.06.16
Published: 2023.06.28

A Study on Modeling and Experiment of a Wave Energy Converter Using Mechanical Coupled with Hydraulic Power Take-Off

Binh Phan Cong[1], Tri Truong Quang[1], Hai Nguyen Le Dang[1], Long Nhut-Phi Nguyen[1*]

[1] Faculty of Mechanical Engineering, HCMC University of Technology and Education (HCMUTE), 1 Vo Van Ngan Street, Linh Chieu Ward, Thu Duc City, Ho Chi Minh City, 71300, Vietnam

* Corresponding author's e-mail: longnnp@hcmute.edu.vn

ABSTRACT

The article's proposal refers to a new concept of wave energy converter (WEC), in which the power take-off (PTO) is combined with the mechanical and hydrostatic transmission. Here, the wave energy is absorbed by turning the two-way movement of an incident wave into the one-way rotation of a hydraulic pump which drives a high-pressure (HP) hydraulic circuit. Electricity is generated using a rotating generator which is driven by an HP hydraulic circuit. First, the coupled PTO mechanism is presented to describe the working principle of the proposed WEC. Next, a mathematical model of the buoy connects generator system is shown to analyze the equipment's performance subjected regular waves. And then, by using the theory of linear potential wave, the hydrodynamic forces acting on the semi-submerged floating buoy and an analytical model of the mechanical transmission coupled with the hydraulic transmission are modeled to investigate the motion of the rotary generator. An experimental Setup is performed to verify the analytical model. Based on the validated model, a structural optimization is calculated to bring the system to resonance condition. Then, a dry test is implemented to analyze the system's performance. Some optimum parameters are determined and applied to the analytical model, which sends the signal to drive the actuator. As a result, the absorbed efficiency is increased significantly.

Keywords: power take-off, mechanical coupled with hydraulic power take-off, hydrostatic transmission, wave energy converter, modeling.

INTRODUCTION

The most urgent duty is to utilize the available sustainable resource to generate electricity to achieve zero emissions by 2050 [1–3]. Renewable energy resources are the potential choice for reaching the goal. Among them, energy from waves shows great potential candidates compared to power from the sun and wind. It is a clean energy supply and can be predictable, persistent, and spatially concentrated [4–5].

The production of electricity from ocean waves (potential and inexhaustible energy source) has attracted particular attention since the first patent on wave energy was published. And since then, many scientists have manufactured devices to harness wave energy. A review article introducing the current WEC technology focusing on the UK or Britain was presented in [6]. Also, the study [7–8] showed the revolution (since the 1970s) in using wave energy was studied, highlighted ideas, and carried out manufacturing and implementation of WEC at sea.

The research [9] recently presented a complete report on WEC technology. Here, the most suitable places for the global resource to be exploited in the WEC are figured out, and the various kinds of them along with their characteristics, are also described in detail. Besides, the improvement of the device measurement during the ocean trials was investigated and applied to typical wave energy conversion technologies [10].

There are numerous WEC technology concepts; however, some of them are more advanced than others. Based on the tendency of companies, the WEC development rating can be shown in [9].

The eight main types of WEC have been identified and shown in [11]. Among these types, the point absorber has got more attention to develop the converters; maybe it is simpler and less expensive than other types. Buoy's size is rather small compared to the wavelength. And the wave energy can be collected in all directions with this type. The generator's rotary or linear motion to generate electricity is transferred from a device's up and down movement under waveform motion.

Based on point-absorber power take-off (PTO) equipment, the three main mechanisms in absorbing wave energy are direct drive, mechanical, and hydraulic. For the direct drive devices, some typical works were presented in [12–16], which directly convert ocean wave energy into electric energy. Publications [17–22] offer the mechanical PTO for converting wave motion as a floating buoy structure. Studies [23–25] show that hydraulic PTOs converted by hydraulic pumps or cylinders achieve a capacity factor of 30–45% when experimented at sea. Among, Falcão *et al.* [23] presented modeling and control of WEC with hydraulic PTO and gas accumulator, and Yang *et al.* [24] studied analysis of the dynamic effect of the heaving body to defend the hydraulic machinery when the floating device is under the extreme sea states.

In some of the power take-offs presented above, hydraulic PTO equipment has proven to be one of the promising solutions for converting wave energy into electricity. It works in one module and connects multiple units to produce electric power with more flexibility. Many existing technologies have shown harmony between complete concepts and working principles. Modeling and dynamic analysis of WEC is also taken into account. Some experiments evaluated these devices [25, 26]. Most of the existing studies have been done by employing the hydraulic cylinder in the PTO. Here, numerous issues, such as equipment failure or friction loss, etc., reduced energy conversion efficiency. For example, Figure 1 [25] illustrates the characteristic curve efficiency of the hydraulic motor. The performance of the motor depends on its speed. This leads to the total conversion efficiencies is not high due to limitations of hydraulic component efficiency, which occurs under low-speed working conditions. To overcome this limitation, a new PTO design consisting of the mechanical mechanism coupled with the hydraulic mechanism is proposed to increase the performance of the WEC. The mechanical mechanism with a large ratio is employed to bring the hydraulic pump to the optimum speed with high efficiency. Consequently, the hydraulic circuit operates in optimum conditions and performs smoothly. Actually, it can be found that the mechanical PTO can work separately, but the combination of multiple units is still a challenge in real conditions. In this case, the hydraulic PTO is the most potential solution to combine multiple units into a large-scale power plant. The high-efficiency mechanical mechanism coupled with the most flexible hydraulic can be a considered solution.

The article poses a newer wave energy converter (WEC) design that PTO combines mechanical and hydrostatic transmission (MHPTO). Here, wave energy absorption follows the conversion basis: the sea waves' two-way motion into the one-way rotation of the hydraulic pump,

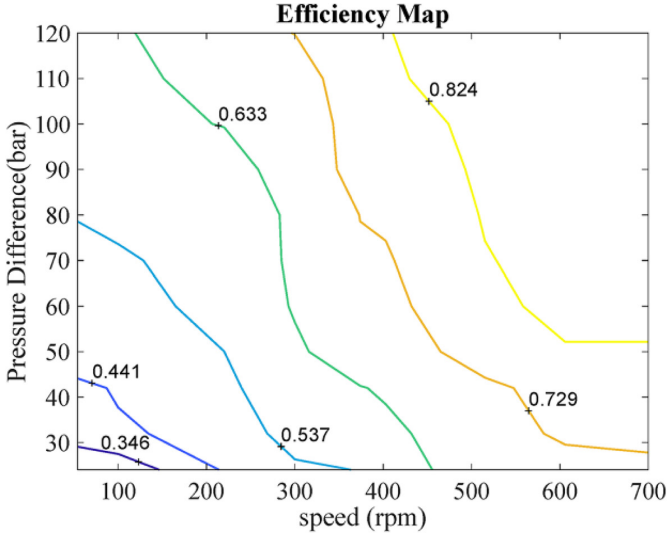

Figure 1. Efficiency map of the hydraulic motor

which drives the high-pressure (HP) hydraulic circuit. Electricity is produced by a radical generator which receives power from HP hydraulic circuit. First, the working principle of WEC is described under the coupled PTO mechanism. Next, the floating buoy-connected generator system's mathematical model is denoted for analyzing the system's performance subjected to regular waves. The linear potential wave theory computes the hydrodynamic forces acting on the semi-submerged floating buoy, and an analytical model of the machine coupled with the hydraulic transmission is modeled to investigate the motion of the rotary generator. An experimental setup is performed to verify the analytical model. Based on the validated model, a structural optimization is calculated to bring the system to resonance condition. Then, a dry test is conducted to assess the system's performance. Some optimum parameters are determined and applied to the analytical model, which sends the signal to drive the actuator. As a result, the absorbed efficiency is increased significantly.

CONCEPTUAL DESIGN & WORKING PRINCIPLE

As illustrated in Figure 2, the equipment configuration comprises three main components: a mechanical device, a hydraulic circuit, and an electric generator.

The mechanical device includes a floating buoy attached to a hemisphere at the lower end, a bidirectional gearbox (BDBG), and a flywheel. Under a tidal wave, the floating buoy must oscillate on the ocean by hydrodynamic forces. Then, the movement of the floating buoy is transferred to the one-direction rotation of the flywheel by the BDBG. As shown in Figure 3, two one-way bearings mounting in the center line of the gears are designed to transmit and amplify the bidirectional motion of the rack into a one-way rotation of the output shaft. Because the output shaft is fixed to the flywheel and drives the hydraulic pump. Consequently, the wave energy from ocean motion is converted to hydraulic energy. Meanwhile, the hydraulic circuit includes an HP gas accumulator, a low-pressure (LP) gas accumulator, a pump, and a motor. The flow from the pressure difference between the HP and LP accumulator drives the hydraulic motor. Moreover, a solenoid valve and a flow control valve control the flow rate into the hydraulic motor to maintain its speed at a desired value.

Finally, a rotation generator is fixed and receives power from the output shaft of the hydraulic motor, and an external load or storage device can take out the generated energy.

Structural optimization and control of the WEC can be done to optimize the energy absorbed. Under specific conventional waves, optimization can be done by generating resonance: making the device's natural frequency close to the wave spectrum's excitation frequency [27]; as a

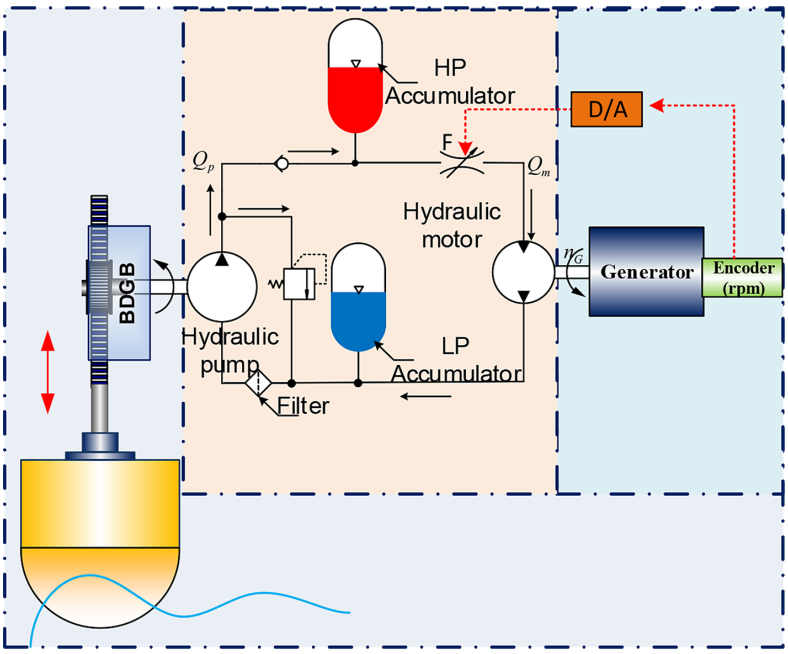

Figure 2. Structure of the introduced WEC

result, almost components in the system are set up to work at the proper speed conditions. Therefore, their efficiencies can be improved significantly. Finally, the overall efficiency of the proposed WEC can reach the highest value.

PTO Model

Mechanical system

The case of regular can be presented as:

$$\eta = A \sin \omega t, (m) \tag{1}$$

The dynamics of the buoy are calculated by solving the set of following equations and applying the law of motion to determine. Combination the incident wave's hydrodynamic forces $F_h(t)$ and the user's force $F_u(t)$ due to the PTO system's load resistance follow as:

$$\begin{aligned} M_{eq}\ddot{z}(t) &= F_h(t) + F_u(t) \\ F_h(t) &= F_e(t) + F_r(t) + F_v(t) + F_s(t) \end{aligned} \tag{2}$$

where: $F_e(t)$ – the excitation force.

The excitation force $F_e(t)$ is calculated as follows:

$$F_e = f_3 \, sin(\omega t + \alpha) \tag{3}$$

where: f_3 – the force amplitude;
α – the phase difference between the wave and the excitation force (use WAMIT, the commercial software, to calculate these coefficients).

The radiation force $F_r(t)$ is expressed in the set of equations:

$$F_r = -m_a\ddot{z} - R_r\dot{z} \tag{4}$$

where: $z(t)$ – the displacement of the buoy;
m_a – the added mass;
R_r – the radiation damping coefficient; these coefficients were obtained by using WAMIT.

The viscous damping force $F_v(t)$ is calculated by:

$$F_v(t) = -\frac{1}{2}\rho C_d A_d(\dot{z} - \dot{\eta})|\dot{z} - \dot{\eta}| \tag{5}$$

where: C_d – coefficient of drag, set one in this research;
A_d – the water plane area of the buoy at rest.

The hydrostatic restoring force $F_s(t)$ is calculated by using the Archimedes principle and is simply given in Eq. 6:

$$F_s = -S_b z \tag{6}$$

where: S_b – so-called the hydrostatic stiffness, which is obtained by Eq. 18 in [18].

Substituting Eq. 3 to Eq. 6 into Eq. 2, the floating buoy dynamic equation can be re-written as:

$$\begin{aligned} F_h(t) = f_3 \, sin(\omega t + \alpha) - m_a\ddot{z} - R_r\dot{z} \\ -\frac{1}{2}\rho C_d A_d(\dot{z} - \dot{\eta})|\dot{z} - \dot{\eta}| - S_b z \end{aligned} \tag{7}$$

As shown in Figure 3, the torque driving the hydraulic pump is calculated as:

$$T_h(t) = \frac{|F_h(t)| \times r_{pi}}{i_{BG}} \tag{8}$$

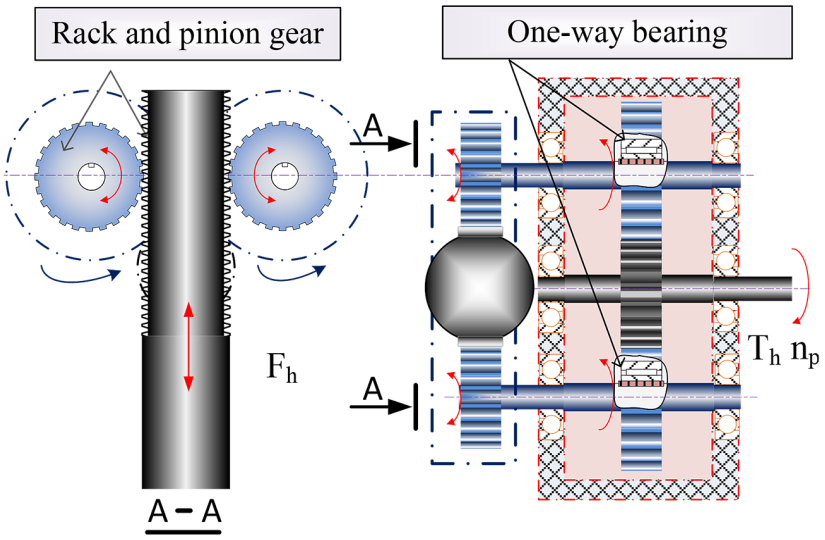

Figure 3. Configuration of the BDGB

where: r_{pi} – the pinion's radius;
i_{BG} – the gearbox ratio

$$n_p = i_{BG} \frac{30000}{\pi r_{pi}} |\dot{z}| \tag{9}$$

Hydraulic circuit

The user's force $F_u(t)$ induced by the hydraulic circuit is obtained in Eq. 10

$$F_u = \frac{T_{hc}}{r_{pi}} \times i_{BG} \tag{10}$$

where: T_{hc} – the reactive torque, which is calculated by the following equation

$$T_{hc} = \Delta p_p \times D_p \tag{11}$$

where: Δp_p – the pressure difference between the outlet and inlet chamber;
Dp – the pump displacement.

As shown in Figure 4, the pump pressure is determined by a continuity Eq. 12

$$\frac{dp_p}{dt} = \frac{\beta}{V_p}(Q_p - Q_r - Q_c) \tag{12}$$

where: β – the bulk modulus, which causes compressible fluid;
V_p – the volume of the pump chamber;
Q_p, Q_c, Q_r – the pump flow rate, flow rate throughout the check valve and the relief valve, respectively.
Here, Q_p – obtained by Eq. 13., Q_c and Q_r – calculated by Eq. 14 and 15, respectively.

$$Q_p = \frac{D_p n_p}{1000} \times {}_p\eta_v \tag{13}$$

where: ${}_p\eta_V$ – the volumetric efficiency of the pump.

$$Q_c = \begin{cases} Q_p - Q_r \; for \; p_c < p_p \\ 0 \; for \; otherwises \end{cases} \tag{14}$$

$$Q_r = \begin{cases} 0 \; for \; p_p \le p_{rset} \\ C_{dis} \dfrac{A_{max}}{p_{reg}} (p_p - p_{rset}) \sqrt{p_p - p_{re}} \end{cases} \tag{15}$$

where: p_p, p_c, p_{rset}, p_{reg} and p_{re} – pump pressure, accumulator inlet pressure, relief valve setting pressure, relief valve regulation pressure, and reservoir chamber pressure, respectively;
C_{dis} – the flow discharge coefficient;
A_{max} – fully open valve passage area. In modeling the gas-charged accumulator, a well-known adiabatic transformation equation of a perfect gas is given by Eq. 16.

$$p_{ga} V_{ga}^n = p_{ga0} V_{ga0}^n \tag{16}$$

where: p_{ga} and p_{ga0} – final and initial pressure;
V_{ga} and V_{ga0} – the final and initial gas volumes in the gas chamber, respectively;
n – the adiabatic coefficient, defined by the ratio of the specific heat. For nitrogen gas, n can be equal to 1.4.

Figure 4 illustrates the fluid pressure at the accumulator inlet is described with the following equations.

$$\frac{dp_c}{dt} = \frac{\beta}{V_c + V_A + V_f}(Q_c - Q_{AH} - Q_m) \tag{17}$$

where: V_c – the volume of the hose from the check valve to the flow control valve;
V_a – the initial volume in the accumulator;
V_f – the entered fluid volume of the high-pressure accumulator and can be calculated in Eq. (18);
Q_{AH} – the fluid flow rate entering the accumulator chamber and can be obtained in Eq. 19

$$V_f = \begin{cases} 0 for p_c \le p_{ga0} \\ V_A \left(1 - \left(\dfrac{p_{ga0}}{p_c}\right)^{\frac{1}{n}}\right) for p_c > p_{P_{ga0}} \end{cases} \tag{18}$$

$$Q_{AH} = \frac{dV_f}{dt} \tag{19}$$

Use the flow control valve to improve performance and make driving the hydraulic motor smooth. The valve works as a variable orifice restriction. The fluid working pressure at the hydraulic motor inlet is determined in the following equation.

$$\frac{dp_m}{dt} = \frac{\beta}{V_m}(Q_m - Q_{mr}) \tag{20}$$

where: V_m – the volume of the motor chamber;
Q_m – the flow rate driving the hydraulic motor is then computed in Eq. 21;
Q_{mr} – the flow rate throughout the motor to the reservoir chamber and is obtained in Eq. 22.

$$Q_m = C_{dis} A_0 \sqrt{(2/\rho)(p_c - p_m)} \quad (21)$$

where: A_0 – the instantaneous orifice passage area; ρ – the fluid density.

$$Q_{mr} = \frac{D_m n_m}{1000} \times {}_m\eta_m \quad (22)$$

where: D_m and ${}_m\eta_m$ – displacement, volumetric and mechanical efficiencies of the hydraulic motor, respectively.

Then, the hydraulic torque T_m is obtained by the following equation:

$$T_m = \frac{\Delta p \times D_m}{20\pi} \times {}_m\eta_m \quad (23)$$

where: $\Delta p = p_m - p_{re}$ (bar) – the difference between motor pressure and reservoir pressure.

Generator model

As shown in Figure 4, the hydraulic motor drives the electric generator to generate electricity. The generator speed is obtained by Eq. 24.

$$I_g \ddot{\theta}_g = T_m - T_g \quad (24)$$

where: T_g – the reactive torque from the generator, which can be modeled in Eq. 25

$$T_g = T_s + T_c + R_g \dot{\theta}_g \quad (25)$$

where: T_S – a static torque;
T_c – a Column's friction torque;
R_g – the electric coefficient, induced by the user's load resistances and taken into account for converting useful power [28].

Then, the output power generated from the electric generator is obtained by the following equation:

$$P_{gen} = \dot{\theta}_g \times T_g \times \eta_g \quad (26)$$

where: η_g – the mechanical efficiency of the electric generator.

Experimental parameters

The first test is to explore the PHPTO's hydrodynamic performance subjected to two different regular waves. It measures the elevation of the buoy, the magnitude of torque as well as the speed of the pump. The simulation results were also plotted in the same figure to compare to the test results. Then, the different values are obtained and shown on the bottom floor of these Figures to validate the model.

Figure 5 depicts the experimental setup performed in the water tank to prepare the tests. A prototype system includes a wave-making machine, the floating buoy combined with BDGB by the rack & pinion, the hydraulic circuit, and a magneto-rheological (MR) brake.

The wave maker was deployed at the Research Institute of Medium & Small Shipbuilding (RIMS), Busan, Korea. Various amplitudes and frequencies of two regular waves are simulated using a wave simulator system to implement the tests. Table 1 presents the parameters of the defined wave.

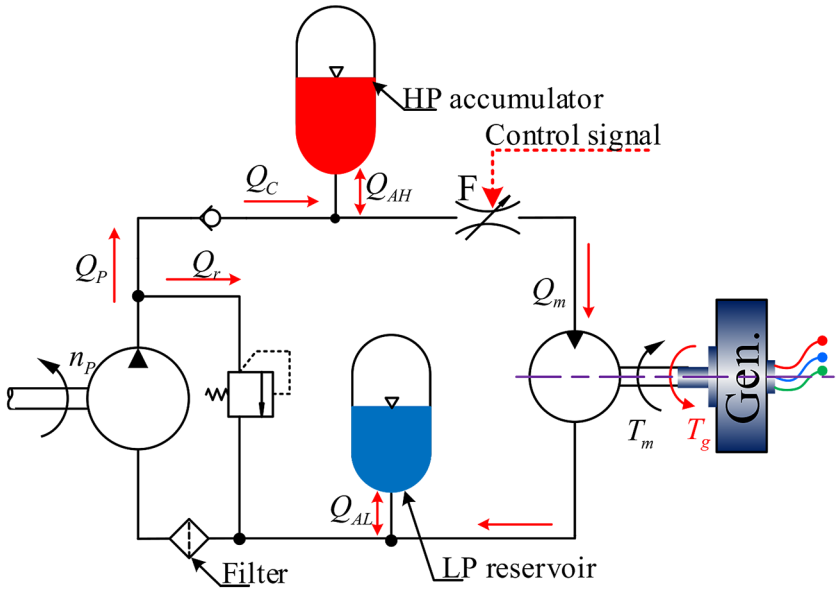

Figure 4. Configuration of the hydraulic circuit

Table 2 describes the defined setting parameters of the PTO.

Table 3 shows the PTO's friction parameters after using MATLAB's curve-fitting tool. The implementation process follows the model of Brian Armstrong in [28] and is presented in [18].

Table 1. Input wave specification

Parameter	Case 1	Case 2
Wave height [m]	H_1 = 0.22	H_2 = 0.13
Angular frequency [rad/s]	ω_1 = 3.7	ω_2 = 2.8
Wave number [rad/m]	k_1 = 1.15	k_2 = 0.89
Depth of water [m]	h_1 = 1.2	h_2 = 1.2

Table 2. The setting parameters of the PTO

Specifications	Parameters
Radius of buoy a [m]	0.6
Estimated draft l_0 [m]	0.385
Total mass of Buoy M_b [kg]	78
Radius of Pinion r_{1pi} [m]	0.05
Ratio of Gearbox i_{GB}	4

Table 3. Setting parameters of the MR brake

Specifications	Parameters
Breakaway friction torque T_{br} [Nm]	0.15
Coulomb friction torque T_c [Nm]	0.1
Transition approximation coefficient c_T [s/rad]	10
Viscous friction coefficient R_f [Nms/rad]	10^{-2}

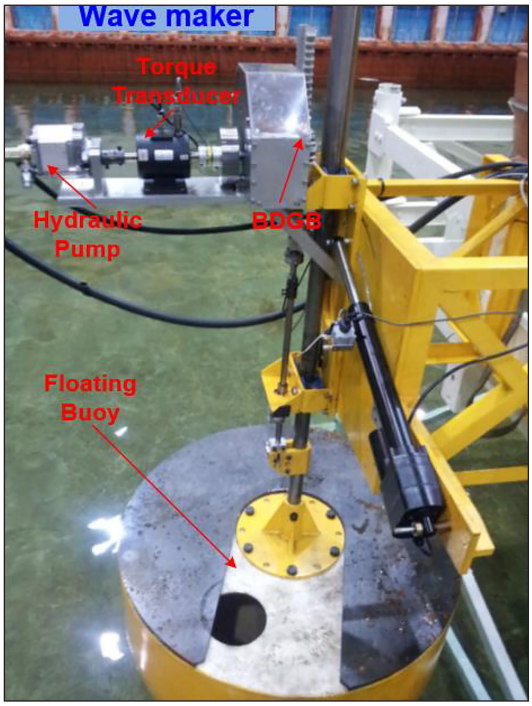

Figure 5. Experiment setup for testing MHPTO

Test performance

The main tests are done to analyze the suggested MHPTO's performance as well as model verification. The tests are carried out under two various regular waves. The wave simulator generates the various amplitudes and frequencies of waves. A feedback control algorithm is applied to the MR brake to generate the reactive torque from

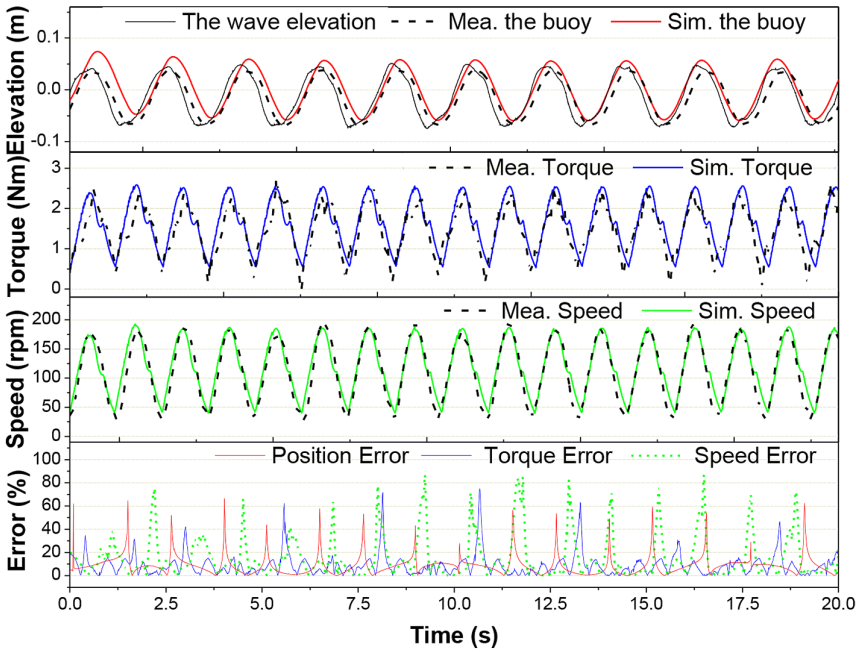

Figure 6. Case 1 – experimental test results

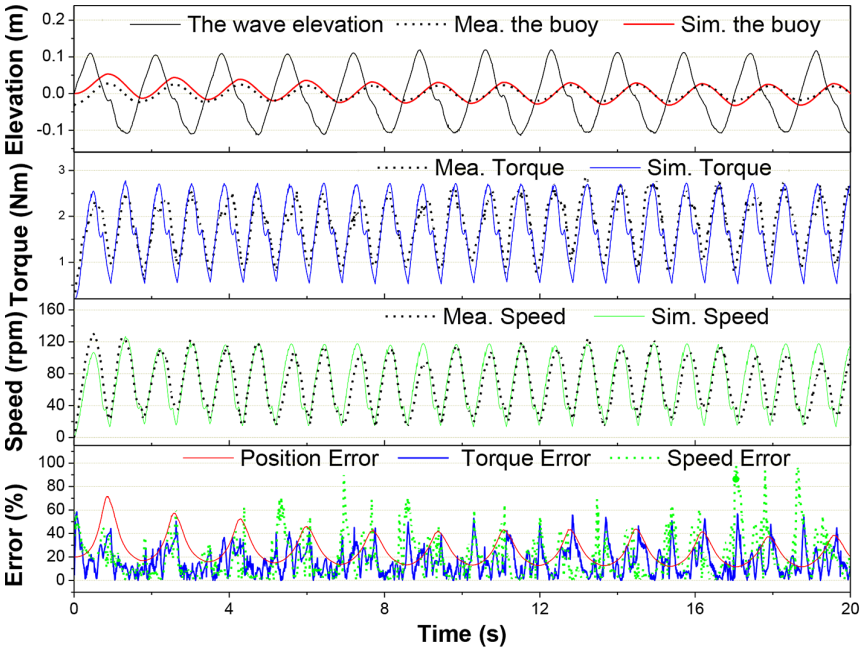

Figure 7. Case 2 – experimental test results

the electric generator performance. As shown in Figure 6-7, the elevation of the wave and the buoy is measured and compared with the modeling on the top floor. The torque transducer was utilized to measure the torque and speed of the hydraulic and plotted on the second floor and third floor, respectively. And then, the difference between the measurement and modeling are obtained and plotted on the bottom floor.

As shown in Figures 6 and 7, the measured values agree well, and the simulation model can be verified in two scenarios of the test. Inspire of some disturbance at the peak of position due to non-linear characteristics of hydrodynamic behavior & the precision in the mechanical structure, the buoy elevation's mean values, the pump torque, and speed are almost the same as the model. Therefore, the model can be verified for application in the following work.

Structural optimization

To analyze the MHPTO's performance subjected a regular wave, a dry test was carried out in the LAB environment. Based on the validated model, some optimized structural parameters were identified to increase the performance. Under the regular wave, the draft of the floating buoy is calculated to optimize the equivalent mass. Consequently, the natural frequency is reduced to the wave frequency, which brings the MHPTO to resonance condition.

The natural frequency of PTO suspended in water is given by:

$$\omega_0 = \sqrt{\frac{S_b}{m_a + M_b}} \tag{27}$$

For the floating truncated vertical cylinder of radius a and a hemisphere at the lower end, the mass of the floating buoy is obtained in the following equation.

$$M_b = \rho\pi a^2 l_0 - \frac{1}{3}\rho\pi a^3 \tag{28}$$

where: l_0 – the draft of the floating buoy and the hydrostatic stiffness $S_b = \rho g\pi a^2$.

To maximum absorbed power ω_0 should be decreased to the proximity of the wave frequencies ω, which brings the system to resonance condition. By substituting Eq. 28 into Eq. 27, the optimization l_0 can be expressed in the following equation.

$$l_0 = \frac{g}{\omega^2} + \frac{a}{3} - \frac{m_a}{\rho\pi a^2} \tag{29}$$

Experimental setup

The objective of the experimental setup is to analyze the performance of the PTO device and evaluate its efficiency. A test rig was assembled in FPMI LAB and shown in Figure 8. It includes a main control center and a complete PTO.

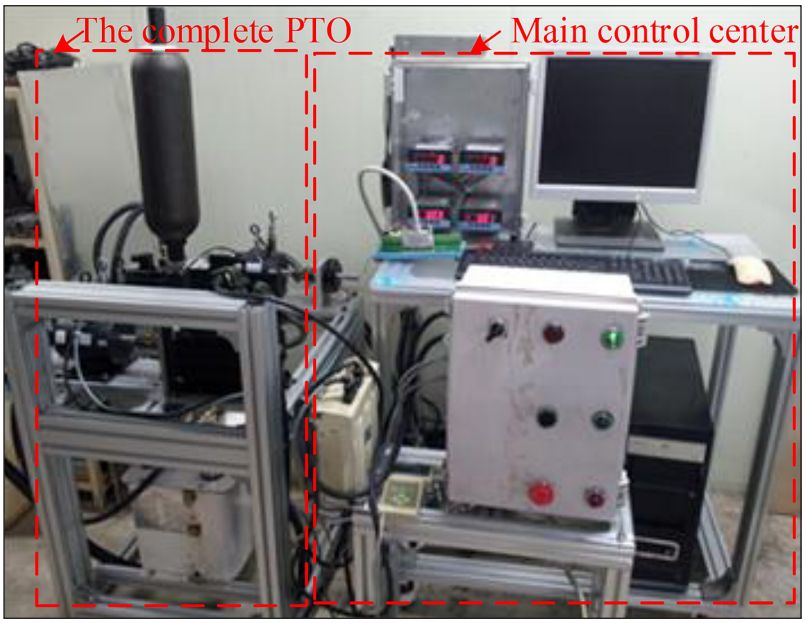

Figure 8. Layout of a dry test rig

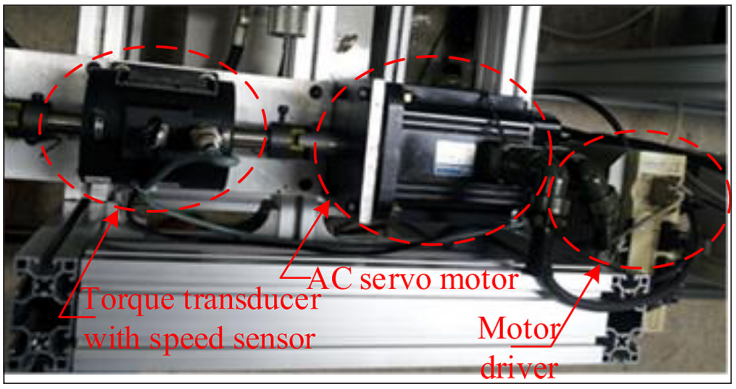

Figure 9. The energy capture device simulation

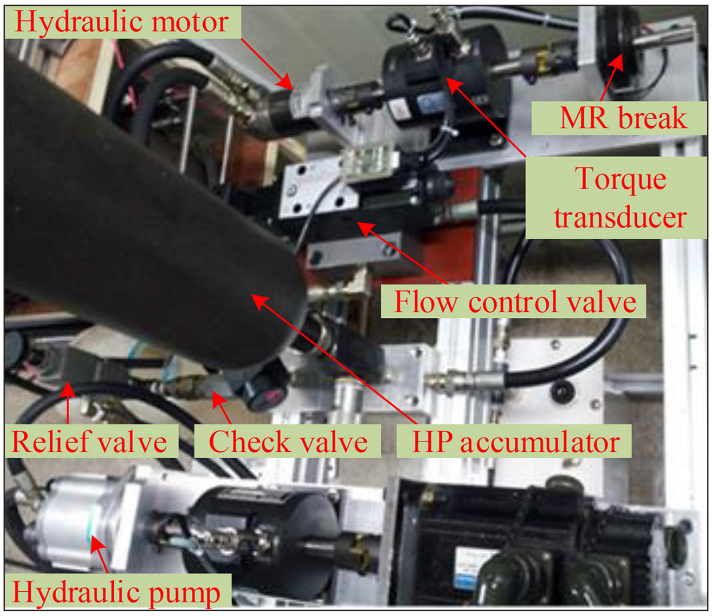

Figure 10. Layout of the hydraulic circuit

The complete PTO system

This system has three main components: an energy capture device, a hydraulic circuit, and an MR brake.

The energy capture device simulates the dynamic performance of the floating buoy and BDGB. Here, an AC servo motor is employed to simulate the behavior of the PTO entrance motion, which drives the hydraulic pump shaft. The servo motor is working in closed loop control with speed feedback in Figure 9. The AC servo motor is used to control the motor's speed based on the command from the main control center. A torque transducer, including a speed sensor, is also assembled between the AC servo motor and hydraulic pump to estimate the absorbed energy.

The hydraulic circuit, along with the MR brake, is assembled and described in Figure 10. Here, a hydraulic pump MB5 (19.0 cm^3/rev) is employed to pump oil from a tank to the hydraulic circuit. A relief valve and check valve are also used to protect the system and to make sure one-way oil flow. An HP accumulator is used as storage energy and supplies oil to the flow control valve, which adjusts the oil flow rate to a hydraulic motor. The hydraulic motor OMM 8 (8.2 cm^3/rev) is coupled with one end of the second torque transducer to estimate generated energy of the system. Finally, an MR brake is fixed to remain at the end of the torque transducer to simulate the generator load.

Main control center

The main control center consists of a PC connected with acquisition card PCI 1711 from Avantech, the speed and torque indicators from SETech, and an electric toolbox in Figure 8. Here, the hydrodynamic behavior of the sea wave and the floating buoy is set up in the Simulink toolbox in Matlab. Then, the command is sent to PCI 1711 to control the operation of the flow control valve and MR brake, and the AC servo motor by means of the electric toolbox. The signal from torque and speed sensors is measured by the PCI card.

Setting parameters for performance test

Prior to tests, some parameters are defined and shown in Table 4. The wave parameters were selected in Table 5. Other parameters using the hydraulic model are based on the Simulink toolbox in Matlab.

Table 4. The PTO's parameters for the simulation

Specifications	Parameters
Radius of buoy *a* [m]	0.6
Estimated draft *L* [m]	1.2
Mass M_{eq} [kg]	565

Table 5. The working condition for the simulation

Specifications	Parameters
Height of wave *H* [m]	0.3
Angular frequency ω [rad/s]	2.244
Wavelength λ [m]	15
Water depth *h* [m]	9

Power conversion efficiencies

A typical process of wave energy transmission is depicted in Figure 11. Here, incident wave energy consists of two sources. The first one is absorbed by oscillating floating bodies and converted to electricity by employing the PTO and an electric generator. The second one is returned to the ocean. In order to investigate the performance of a WEC, wave energy, absorbed energy, and output energy must be obtained in the following procedure.

Firstly, the wave power is calculated by the set of equations [27]:

$$P_w = Ec_g, (kW/m)$$
$$E = E_k + E_p = \frac{1}{8}\rho g^2 H^2, (J/m^2) \quad (30)$$

where: E – the mean wave energy density per unit horizontal area, the sum of kinetic E_k and potential energy E_p;
c_g – the group velocity, which can be obtained, for constant water depth h, in the set of equations:

$$c_g = \frac{D(kh)}{2\,tanh(\,kh)} c_p = \frac{g}{2\omega} D(kh)$$
$$D(kh) = \left[1 + \frac{2kh}{sinh(\,2kh)}\right] tanh(\,kh) \quad (31)$$

where: $D(kh)$ – the depth function;
k – the angular repetency (wave number), is determined as follows: $k = 2\pi / \lambda$.

Secondly, the absorbed power (the captured power) is given in [27] by the following equation:

$$P_{ab} = \frac{1}{2} R_{eq} \dot{z}^2 \quad (32)$$

where: R_{eq} – the equivalent external damping of the PTO device.

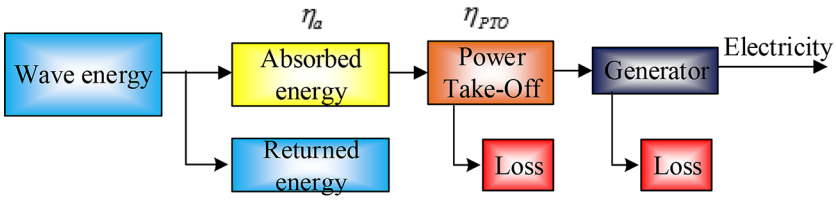

Figure 11. Wave power transmissions and absorption efficiencies

However, for simplicity in the experiment, absorbed energy can be measured by multiplying the torque and speed of the hydraulic pump input shaft and expressed in Eq. 33

$$P_a \approx \frac{T_{hc} \times n_p}{0.975}, [W] \tag{33}$$

Finally, the generator energy of the PTO device used to operate the electric generator can be obtained by the following equation:

$$P_g \approx \frac{T_g \times n_g}{0.975}, [W] \tag{34}$$

The absorbed energy efficiency (the capture width ratio) is defined as the ratio of absorbed energy P_a and incident wave energy P_w in the following equation:

$$\eta_a = P_a / P_w \tag{35}$$

The following equation defines PTO efficiency as the ratio of PTO energy to absorbed energy:

$$\eta_{PTO} = P_g / P_a \tag{36}$$

The following formula describes the total efficiency (37)

$$\eta_o = \eta_o \times \eta_{PTO} = P_g / P_w \tag{37}$$

EXPERIMENTAL RESULTS

Multiple simulations are carried out with the parameters of a regular wave shown in Table 2. Then, the result is sent to control the AC servo motor. The data is obtained and plotted in Figure 12 and Figure 13. As shown in Figure 12, from 15 s, the buoy position is in stability and closed to waveform due to the resonance behavior of the system. The torque and speed of the generator are measured and compared with that the simulation results. It is indicated that the modeling can be validated by agreement between simulation and experiment results. In Figure 13, the wave energy is calculated and compared with the generated energy of (PTO) and absorber energy. Finally, the efficiency is obtained and shown at the bottom of this figure. It is nearly about 50% PTO efficiency and 36% overall efficiency.

CONCLUSION

This article shows the newest concept for the energy extraction of ocean waves. A combination between hydrodynamic and MHPTO based on the time domain using pre-computed hydrodynamic coefficients is used to investigate the system's performance. Then, the experiment setup is done to measure and record the torque and speed. An analysis of the induced torque, speed, and generated energy shows that the mathematical model and the experimental data agree reasonably. Additionally, the efficiencies of the WEC were

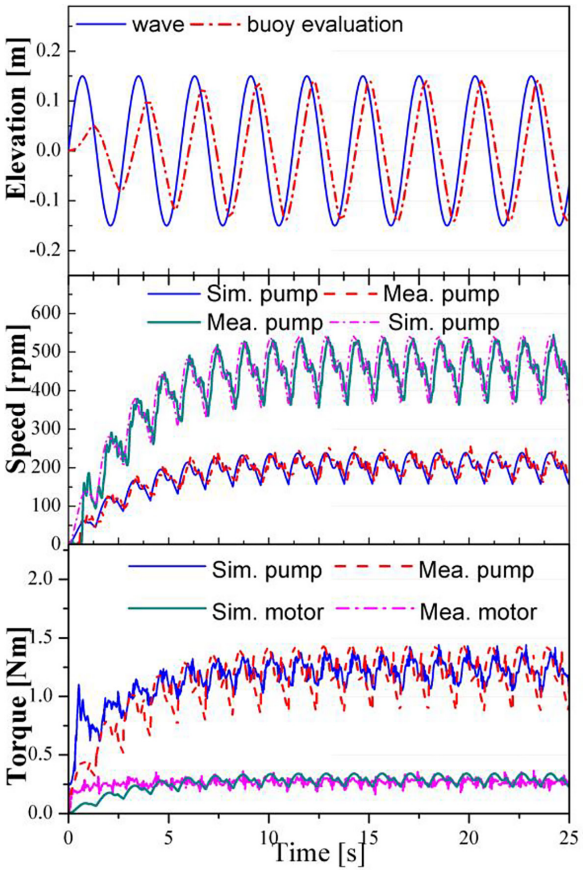

Figure 12. Speed and torque comparison

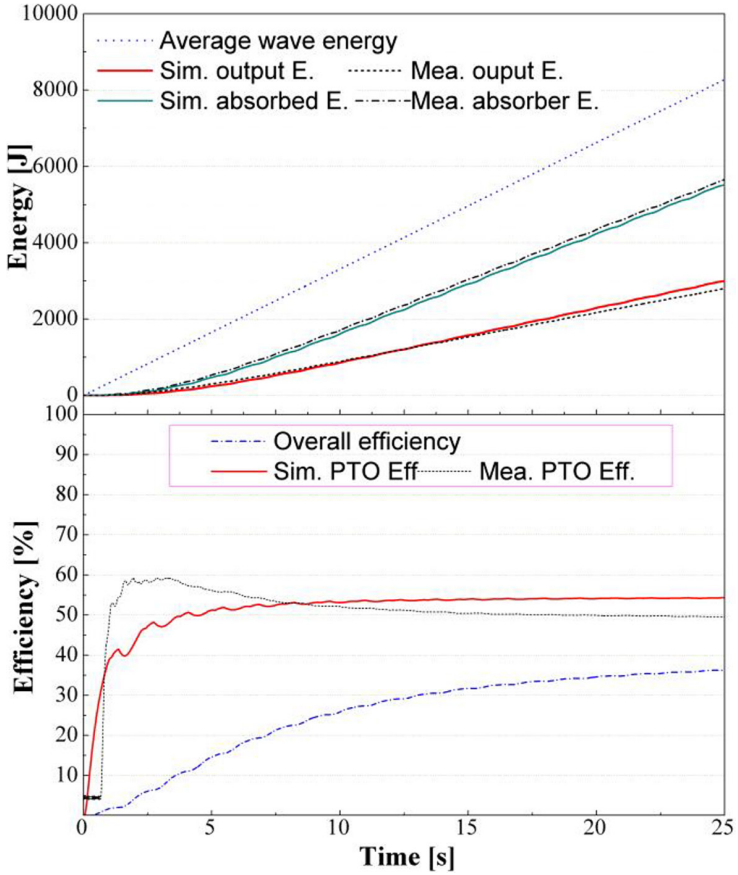

Figure 13. Energy and efficiency comparisons

calculated using the mean incident wave power, the absorbed power, and the generated power. The proposed WEC can achieve a capture width ratio of 50 and an overall efficiency of 36.

Acknowledgements

This work belongs to the project grant No: T2022-90 funded by Ho Chi Minh City University of Technology and Education, Vietnam.

REFERENCES

1. Guterres, A. Carbon Neutrality by 2050: the World's most urgent mission. (United Nations Secretary General, 2020.) https://www.un.org/sg/en/content/sg/articles/2020-12-11/carbon-neutrality-2050-theworld%E2%80%99s-most-urgent-mission (2020). Accessed 10 Feb 2021
2. Badran, A.A., Obeidat, F.A. 2022. Solar hot water heating and electricity generation using PV/T hybrid system. Journal of Ecological Engineering, 23(5), 196–206. https://doi.org/10.12911/22998993/146783
3. Hassan, K.A. 2022. Generating electricity from soil using different sources of manure. Journal of Ecological Engineering, 23(8), 187–192. https://doi.org/10.12911/22998993/150721
4. Rusu, E., Onea, F. 2018. A review of the technologies for wave energy extraction. Clean Energy, 2(1), 10–19.
5. Guo, B., Ringwood J.V. 2021. A review of wave energy technology from a research and commercial perspective. Renewable Power Generation, IET. September 2021.
6. Falnes, J. 2007. A review of wave-energy extraction. Marine Structures, 20, 185–201.
7. Drew, B., Plummer, A.R., Sahinkaya, M.N. 2009. A review of wave energy converter technology.
8. Anto´nio, F., de Falca˜o, O. 2010. Wave energy utilization: A review of the technologies. Renewable and Sustainable Energy Reviews, 14, 899–918.
9. López, I., Andreu, J., Ceballos, S., de Alegría I.M., Kortabarria, I. 2013. Review of wave energy technologies and the necessary power-equipment. Renewable and Sustainable Energy Reviews, 27, 413–434.
10. Lindroth, S., Leijon, M. 2015. Offshore wave power measurements – A review. Renewable and Sustainable Energy Reviews, 15, 4274–4285.
11. European Marine Energy Centre (EMEC). Wave Devices. http://www.emec.org.uk/marine-energy/

wave-devices/ (August 2017, date last accessed).

12. Binh, P.C., Truong, D.Q., Ahn, K.K. 2012. A study on wave energy conversion using direct linear generator. Proc. of 12th International Conference on Control, Automation and Systems.
13. Leijon, M., Bernhoff, H., Agren, O., et al. 2005. Multiphysics simulation of wave energy to electric energy conversion by permanent magnet linear generator. IEEE Trans. on Ener. Conv., 20(1), 219–224.
14. Colli, V.D., Cancelliere, P., Marignetti, F, et al. 2006. A tubular-generator drive for wave energy conversion. IEEE Trans. on Ind. Elec., 53(4), 1152–1159.
15. Binh, P.C., Nam, D.N.C., Ahn, K.K. 2015. Design and modeling of an innovative wave energy converter using dielectric electroactive polymers generator. International Journal of Precision Engineering and Manufacturing, 16(5), 945–955.
16. Binh, P.C., Ahn, K.K. 2016. Performance optimization of dielectric electro active polymers in wave energy converter application. International Journal of Precision Engineering and Manufacturing, 17(9), 1175–1185.
17. Ahn, K.K., Truong, D.Q., Tien, H.H., Yoon, J.I. 2011. An innovative design of wave energy converter, Renewable Energy, 1–9.
18. Binh, P.C., Tri, N.M., Dung, D.T., Ahn, K.K., Kim, S.J., Koo, W. 2016. Analysis, design and experiment investigation of a novel wave energy converter. IET Generation, Transmission and Distribution, 10(2), 460–469.
19. Tri, N.M., Binh, P.C., Ahn, K.K. 2018. Power take-of system based on continuously variable transmission confguration for wave energy converter. International Journal of Precision Engineering and Manufacturing-Green Technology, 2018, 5(1), 89–101.
20. Dung, D.T., Binh, P.C., Ahn, K.K. 2019. Design and investigation of a novel point absorber on performance optimization mechanism for wave energy converter in heave mode. International Journal of Precision Engineering and Manufacturing-Green Technology, 6, 477–488.
21. Dung, D.T., Tri, N.M., Binh, P.C., Ahn, K.K. 2019. Development of a wave energy converter with mechanical power take-of via supplementary inertia control. International Journal of Precision Engineering and Manufacturing-Green Technology, 6, 497–509.
22. Dung, D.T., Binh, P.C., Ahn, K.K. 2019. Modeling and experimental investigation on performance of a wave energy converter with mechanical power take-of. International Journal of Precision Engineering and Manufacturing-Green Technology, 6, 751–768.
23. Falcão de, O.A.F. 2007. Modelling and control of oscillating-body wave energy converters with hydraulic power take-off and gas accumulator. Ocean Engineering, 34(14–15), 2021–2032.
24. Yang, L., Hals, J., Moan, T. 2010. Analysis of dynamic effects relevant for the wear damage in hydraulic machines for wave energy conversion. Ocean Engineering, 37(13), 1089–1102.
25. Dung, D.T., Cuong D.T., Ahn, K.K. 2021. Experimental assessment of the power conversion of a wave energy converter using hydraulic power take-of mechanism. International Journal of Precision Engineering and Manufacturing-Green Technology, 8, 1515–1527.
26. Thinh, D.H., Truong, D.Q., Tri, N.M, Binh, P.C., Dung, D.T, Seyoung, L., Hyung-Hyu P., Ahn K.K. 2017. Proposition and experiment of a sliding angle self-tuning wave energy converter. Ocean Engineering, 1–10.
27. Falnes, J. 2002. Ocean waves and oscillating systems, linear interaction including wave-energy extraction. U.K.: Cambridge Univ.
28. Armstrong, B., de Wit, C.C. 1995. Friction modelling and compensation. The control handbook (CRC Press, 1995).